Stress reduction in tungsten films using nanostructured compliant layers

Tansel Karabacak
Department of Physics, Applied Physics, and Astronomy, Rensselaer Polytechnic Institute, Troy, New York 12180-3590

Catalin R. Picu
Department of Mechanical, Aerospace and Nuclear Engineering, Rensselaer Polytechnic Institute, Troy, New York 12180-3590

Jay. J. Senkevich, Gwo-Ching Wang, and Toh-Ming Lu
Department of Physics, Applied Physics, and Astronomy, Rensselaer Polytechnic Institute, Troy, New York 12180-3590

(Received 14 January 2004; accepted 11 August 2004)

The residual stress in thin films is a major limiting factor for obtaining high quality films. We present a strategy for stress reduction in sputter deposited films by using a nanostructured compliant layer obtained by the oblique angle deposition technique, sandwiched between the film and the substrate. The technique is all *in situ*, does not require any lithography steps, and the nanostructured layer is made from the same material as the deposited thin film. By using this approach we were able to reduce stress values by approximately one order of magnitude in sputter deposited tungsten films. These lower stress thin films also exhibit stronger adhesion to the substrate, which retards delamination buckling. This technique allows the growth of much thicker films and has enhanced structural stability. A model is developed to explain the stress relief mechanism and the stronger adhesion associated with the presence of the nanostructured compliant layer. © *2004 American Institute of Physics*. [DOI: 10.1063/1.1803106]

I. INTRODUCTION

The control of mechanical stress in technologically important thin films deposited by the sputter deposition technique has attracted significant attention. The thin film stress often determines the limit of film thickness without cracking, buckling, or delamination,[1–6] as well as electrical[7–9] and optical properties, and distortions in x-ray masks.[10]

Haghiri-Gosnet *et al.*[11] and Windischmann[12] showed that the intrinsic stress in sputtered tungsten films is correlated to Thornton's structure zone model (SZM).[13–17] The SZM relates the microstructure of sputtered thin films to the most prominent deposition parameters such as working-gas pressure and substrate temperature. It has been shown that the transition from zone *I* of porous and columnar structure to zone *T* of a denser film (e.g., by passing from high to lower working-gas pressures) corresponded to a dramatic change of stress from high tensile to high compressive values (i.e., from a few GPa tensile to a few GPa compressive for tungsten). The rapid change of stress with pressure allows only a narrow window of pressures that yields reasonably low-stress values (i.e., smaller than few hundred MPa for tungsten). Therefore, obtaining low-stress films by controlling the working-gas pressure (at a fixed pressure during deposition) has been difficult and is not a robust method.[11] In the high-pressure part of zone *I* it is possible, but difficult, to produce low-stress films. These films exhibit poor electrical properties due to their columnar microstructure. In addition, the stress of these films evolves in time partially due to adsorbed oxygen in the voids, which leads to compressive stresses.[11] Similarly, the stress is a sensitive function of the dc bias voltage[8] and substrate temperature[11,18] near the transition between tensile and compressive values. Again this makes stress control difficult when low tensile or compressive values are desired.

A rf-substrate biasing technique was shown to improve the stress control over an optimum region of the cathode current, pressure, and the rf-substrate bias values.[8] However, the method is sensitive to the material type to be deposited, and finding the optimum parameter space can be challenging.

Maier *et al.* studied the effect of plasma-etch surface treatment of graphite substrates before deposition on the adhesion properties of tungsten films sputter deposited at various temperatures.[6] The maximum film thickness without delamination, at high deposition temperatures ($\geqslant$400 °C), was $\sim$1 μm without, and $\sim$3 μm with plasma pretreatment. However, the plasma treatment is a chemical method limited to certain types of substrates and materials to be deposited. Also, deposition may require elevated substrate temperature.

A recently developed technique, "nanoheteroepitaxy," was shown to be a promising method to obtain thicker epitaxial films with lower strain energies.[19–21] Nanoheteroepitaxy requires the deposition of an epilayer on a compliant patterned substrate of nanoscale islands. The epilayer grows only on the islands at initial times, while a continuous film develops at later times through a coalescence process. Although nanoheteroepitaxy is specific to epitaxial films and needs costly lithographic steps for island formation, it may also lead to an approach to stress reduction in sputter deposited thin films.

In the present work, we propose a similar method which does not require patterning and which may be used with a large variety of materials and substrates. In this method, a

nanostructured compliant layer (NCL) obtained by a self-assembling growth mechanism is deposited between the actual film and the substrate. The layer is obtained in a single processing step and is made from the same material as the film. The stress reduction effect is obtained in all cases in which the NCL exists, independent of the deposition parameters like pressure, temperature, and substrate biasing. The layer is grown by the oblique angle deposition technique, while the film is grown by the regular method.

Oblique angle sputter deposition (OASD) was recently shown to be an effective method for fabricating nanostructures of various shapes (i.e., nanorods, nanosprings, etc.) and sizes (i.e., from a few nanometer up to a few hundred nanometers diameter) by a physical self-assembly mechanism.[22–24] The method is simple, easy to implement, all *in situ*, and can be applied to any material that can be vaporized. In the OASD the incident flux of sputtered material impinges on a tilted substrate. The incident particles preferentially attach to the taller surface features resulting in the growth of slanted nanocolumns. Also, if the substrate is rotated during deposition, with the rotational axis perpendicular to the substrate, vertical nanocolumns can be grown.

Once the nanostructured compliant layer is grown by OASD, the angle of incidence is changed to normal incidence *in situ* in order to deposit the usual continuous dense layer of material. It is shown that the compliant layer relieves the stress in the continuous thin film and effectively improves the adhesion, which results in larger critical thickness for delamination buckling, and higher quality films. The process can be repeated to form multilayer films with very large thickness.

II. EXPERIMENT

A dc magnetron sputtering system was used to deposit the W films. The substrate was oxidized *p*-Si(100) (resistivity 12–25 Ω cm) wafers (diameter 7.6 cm). The deposition was performed from a 99.95% pure W cathode of diameter 7.6 cm. The substrates were mounted on the sample holder located at a distance of about 15 cm from the cathode. In the oblique angle deposition, the substrate is tilted so that the angle θ between the surface normal of the target and the surface normal of the substrate can be large. In our case, the angle was either 85° (for nanorods) or 50° (for continuous films). In the normal incidence sputter deposition the tilt angle was set to 0°. The base pressure of 2×10^{-6} Torr was achieved using a turbo-molecular pump backed by a mechanical pump. In all the deposition experiments, the power was 200 W at an ultrapure Ar pressure of 2.0 mTorr. The deposition rates were measured to be 12 nm/min for normal incidence deposition, 11 nm/min at $\theta=50°$, and 5 nm/min at $\theta=85°$. The thickness of the films was determined with a step profilometer and was verified by cross-sectional scanning electron microscopy (SEM).

The maximum temperature of the substrate during the deposition was measured to be 85 °C. It was previously shown that a 50 °C increase in substrate temperature during sputter deposition of tungsten leads to a negligible "thermally induced" stress value of ~50 MPa.[7] Therefore, the large stresses reported here are mostly due to stress production during film growth rather than to the thermal expansion coefficient mismatch.

The measurement of the intrinsic film stress was performed by using a dual wavelength ($\lambda_1=670$ nm and $\lambda_2=750$ nm) Flexus 2320 system based on the wafer curvature technique. The average film stress σ then was calculated using Stoney's equation[25]

$$\sigma = \frac{1}{6R}\frac{E}{(1-\nu)}\frac{{d_{sub}}^2}{d}, \tag{1}$$

where E, ν, and d_{sub} are Young's modulus, Poisson's ratio, and the thickness of the substrate, respectively, and d is the film thickness (assuming $d \ll d_{sub}$). If R_1 and R_2 are the radii of curvature of the reference wafer before and after deposition, the relative substrate radius of curvature R may be calculated as $R=R_1R_2/(R_1-R_2)$. In this notation, the negative and positive signs of stress correspond to tension and compression, respectively. Also, when a multilayer structure of W-film/NCL/Si-wafer is grown with a NCL carrying negligible stress, the stress in each layer is computed by taking the current NCL/Si-wafer structure as the reference substrate (E, ν, and d_{sub} are approximated as those of the Si wafer). This is equivalent with approximating that the curvature of the substrate is due to each film in the multilayer structure as if it were alone on the substrate, and their contribution is additive.[26]

The surface topography was investigated using optical and atomic force microscopy (AFM). We used a contact-mode AFM (Park Scientific Auto CP) with a Si tip of radius ~10 nm, and side angle 12°. The scan sizes were 2×2 μm^2 with resolution of 512×512 pixels. The root mean square (rms) roughness was extracted from the quantitative surface height values.

The scotch-tape peel test was used to obtain a qualitative indication of film adhesion.

III. RESULTS AND DISCUSSION

We first studied the evolution of stress and adhesion properties of W films deposited on silicon wafers at normal incidence with no compliant layer being present. The films were observed to delaminate and peel off once thicker than 120 nm. Figure 1(a) shows an optical microscopy topography of the delaminated W film. Similar delamination buckling patterns were observed before in such films[2,3] and were associated with the presence of high compressive residual stresses.

To relieve the stress, we fabricated a NCL using the OASD technique. We deposited W films on Si wafers tilted at a high angle of $\theta=85°$ with no substrate rotation. The shadowing effect led to the growth of the slanted tungsten nanorods shown in Fig. 2. The thickness of the NCL in Fig. 2 is about 650 nm. The actual NCL used in the present study was fabricated by the same technique but had a much smaller thickness of 50 nm. Due to its porosity, the compliant layer did not carry intrinsic stresses (-3.8 ± 5.2 MPa). A continuous W film was then grown on the NCL substrate at normal incidence, and it was observed that the critical thickness for

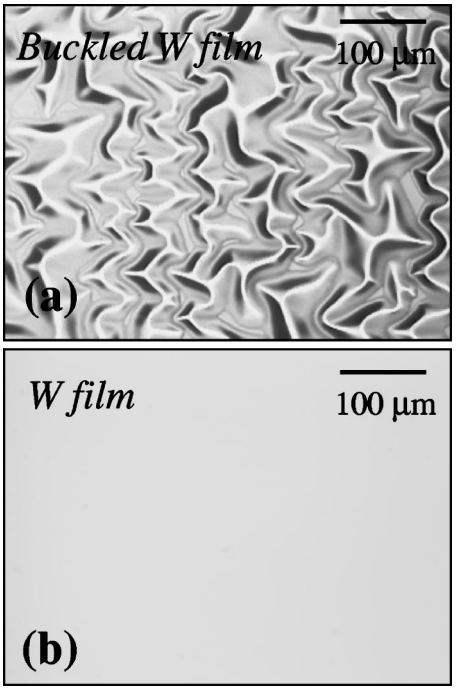

FIG. 1. Optical microscopy images of tungsten film morphologies: (a) A ~240 nm thick W film deposited on a bare Si substrate. Intense buckling occurs. (b) A ~240 nm thick W film deposited on a nanostructured compliant layer (NCL) formed by slanted W nanorods (~50 nm thick and the tilt angle $\alpha \approx 50°$ as measured from the substrate). The film is smooth (rms $= 0.87 \pm 0.05$ nm) and has a good adhesion.

buckling increased to ~500 nm (almost four times the critical thickness of the film without the NCL). An example is shown in Fig. 1(b), where a smooth 240 nm thick W film (rms $= 0.87 \pm 0.05$ nm) deposited on NCL is shown. This must be compared with the film of similar thickness but without the compliant layer shown in Fig. 1(a). The effect of NCL on improving film stability is immediately obvious.

Figure 3 shows the measured stress as a function of film thickness for films deposited on bare Si wafers and on NCL. All stresses in the figure are compressive. The W film with no compliant layer quickly develops a large compressive stress (e.g., ~2.3 GPa at thickness ~25 nm). On the other hand, at the same film thickness (25 nm), the stress in the W film deposited on NCL is approximately one order of magnitude lower. We note that a continuous W film on NCL nanorods develops only after the film reaches a thickness of ~10 nm as observed from SEM images (not shown here). At thicknesses smaller than 10 nm the W film is in the form of isolated islands due to the roughness of the underlying deposition surface. This threshold depends on the thickness of the NCL, as discussed in the following section. Importantly, all W films deposited on NCL (Fig. 3) passed the scotch-tape peel test, which indicates an enhancement in adhesion compared to the no-NCL case.

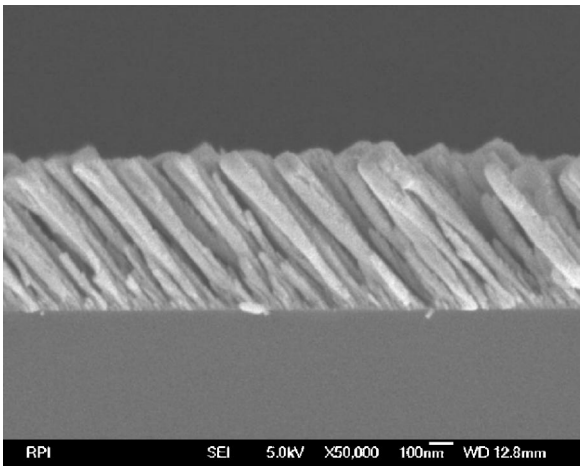

FIG. 2. A SEM image of slanted W nanorods fabricated by oblique angle sputter deposition (OASD). The thickness is ~650 nm. The actual nanostructured compliant layer (NCL) that we used for our study is only ~50 nm thick. The scale bar is 100 nm.

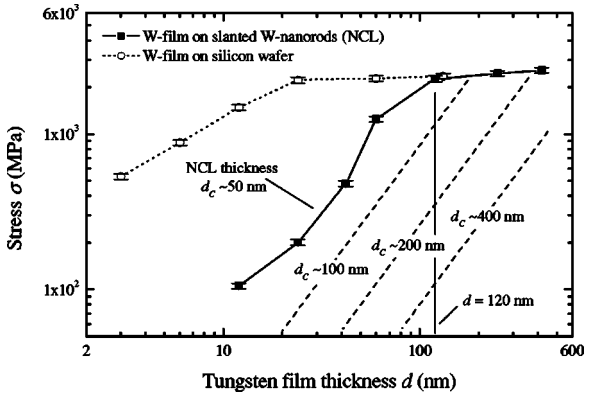

FIG. 3. Log-log plot of the stress in the W film vs the film thickness. The open circles correspond to depositions *without* a nanostructured compliant layer (NCL). Filled squares represent the stress data for W films deposited on NCL of slanted W nanorods ($d_c \sim 50$ nm thick). The dashed lines represent the variation of stress with the film thickness for other values of NCL thickness d_c (100 nm, 200 nm, and 400 nm) as predicted by the model. The vertical line is at the film thickness $d = 120$ nm.

The issue of the optimal thickness of the NCL layer was considered next. To this end, we prepared specimens in which the thickness of the film was kept constant (120 nm) and the thickness of the NCL was varied. The residual stress in the film as a function of the NCL thickness is shown in Fig. 4. It is seen that no stress reduction is obtained for very thin NCL layers (2.3 GPa), while when the layer thickness increases to $d_c = 400$ nm, the stress was negligible (90 MPa).

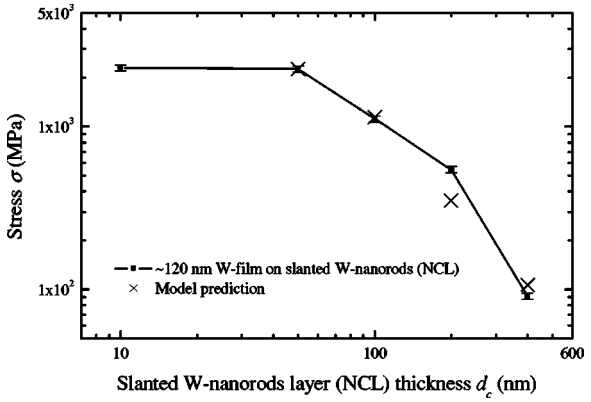

FIG. 4. Variation of the measured stress (filled squares) in 120 nm thick W films as a function of the NCL thickness d_c. The crosses are obtained from the intercepts of the predicted stress lines (dashed lines) with the vertical line representing a film thickness $d = 120$ nm in Fig. 3.

In addition, the possibility of growing very thick tungsten films by alternating NCL and continuous W layers was investigated. For this, we used an *in situ* controller to change the tilt angle θ of the substrate such that at high θ we obtain the NCL, while at low θ a continuous film results. Figure 5(a) shows an optical micrograph of a continuous 550 nm thick W film which, as expected, is heavily buckled. Then, the film was deposited in the multilayer form, with continuous W films of thickness 550 nm separated by NCLs of thickness 50 nm. Up to six layers (i.e., three layers of W film and three layers of NCL) were deposited such that the total thickness of the multilayer was ~1800 nm. See Fig. 5(c). The film is relatively smooth (rms=14.0±0.5 nm) and no delamination was observed. See Fig. 5(b). In addition, the film passed the peel test and had a very low stress of σ =384.1 MPa.

IV. THE MODEL

The most relevant experimental observations can be summarized as follows.

(1) The stress in a very thin film deposited on NCL is significantly lower than that in the film without NCL (initial growth stages).

(2) As the thickness increases, the stress increases in both types of films following a power law with roughly the same exponent (see slope of rising part of the curves in Fig. 3). Therefore, the stress production mechanism should be similar in the two cases.

(3) Both types of films reach the same maximum stress of 2.3 GPa (at different film thicknesses).

(4) W films with NCL buckle at a larger film thickness (e.g., W films with 50 nm NCL buckled at $d \approx 500$ nm compared to $d \approx 120$ nm, for W films without NCL).

These observations suggest that the effects of the NCL are (a) to delay the inception of stress buildup, and (b) to toughen the interface such that delamination buckling occurs at higher levels of strain energy stored in the film (larger film thickness). In the following, we consider each of these effects and present a conceptual model for their justification.

A. The effect of roughness

During initial stages of growth, thin films conform to the topology of the nanorods. Since the surface on which the film grows (top surface of the NCL) is rough, the film is wavy as long as its thickness is smaller than the roughness [Fig. 6(a)]. Let us consider the example of a wavy thin film of thickness smaller than the amplitude of the wave it describes and which initially carries no residual stress. Let us apply to the film a transformation strain (eigenstrain) equivalent to the residual strain that would develop during growth in a flat film. While the flat film is constrained and can only relax by buckling (assuming that the substrate is rigid and there is no stress driven diffusion), the wavy film can easily relax the eigenstrain by out-of-plane displacement. The out-of-plane relaxation (out of the plane of the wafer surface, but within the plane of the wavy film) is not constrained by the substrate. This mechanism is effective when the film thickness is smaller than half of the wavelength of its waviness. Once the two measures become similar, the mechanism ceases to be effective and stress starts building up in the film. It is possible to estimate the average waviness of the film at

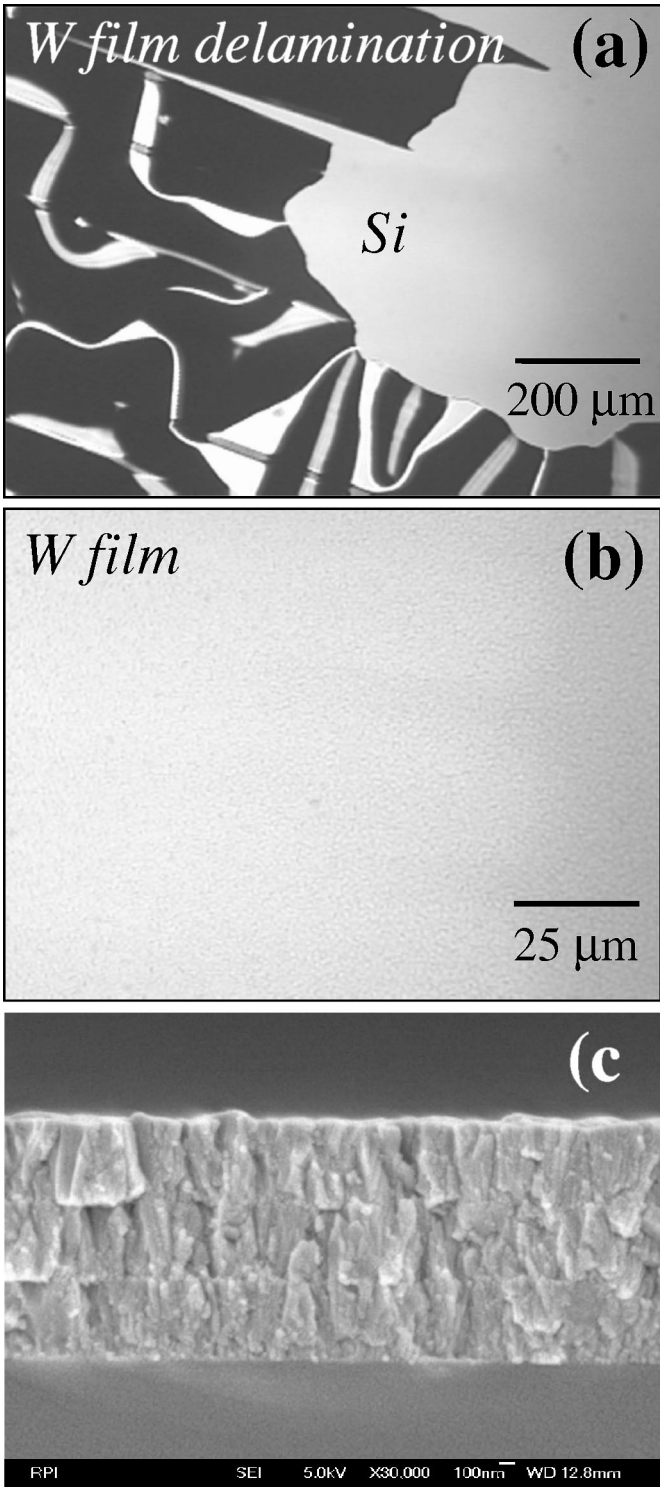

FIG. 5. (a) Top view (optical microscopy image) of a continuous 550 nm thick W film deposited on a bare Si substrate at oblique angle θ=50°. Extreme peeling is observed. (b) Top view (optical microscopy image) and (c) cross-sectional SEM image of a multilayer (composed of six layers) W film in which NCL layers of 50 nm thickness are intercalated between continuous films 550 nm thick. The total film thickness is ~1800 nm. No delamination is observed and the surface rms roughness is 14.0±0.5 nm. The scale bar is 100 nm.

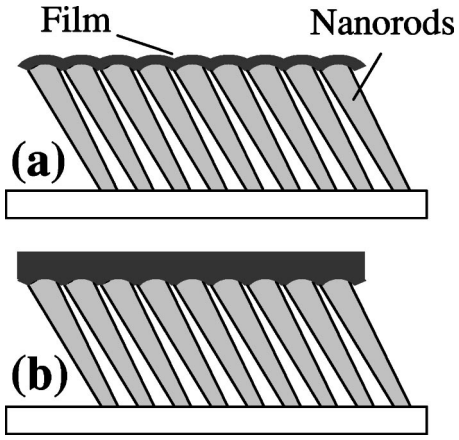

FIG. 6. Schematic representations of two stages during film growth on NCL. (a) When the film is very thin, it conforms to the roughness of the surface on which it is deposited. As long as the thickness is smaller than the roughness (or the waviness of the film), no significant stress builds up in the film due to the limited geometric constraint. (b) Once the film grows thicker, its surface becomes flat and the constraint is similar to that in a continuous film.

its incipient growth stages by measuring the roughness of the top surface of the NCL. A roughness of ~10 nm was measured for the NCL of 50 nm thickness. Along the line of reasoning discussed here, this would suggest that stress buildup in the film should be observed only after the film is ~10 nm thick. This is in excellent agreement with the data presented in Fig. 3. In fact, as observed above, the film is discontinuous when its thickness is thinner than 10 nm.

As the NCL thickness increases, its roughness increases. This is due to the nonuniform growth of the nanorods. On this unpatterned substrate, the nanorods nucleate at high density (number of rods per unit area). They initially have diameters on the order of 5–10 nm. As they grow, their diameter increases slightly, while their density decreases. Therefore the roughness of the top surface of the NCL increases and is on the order of the average nanorod diameter. Specifically, the roughness values (i.e. ~ average nanorod diameter) measured for the 50, 100, 200, and 400 nm thick NCLs are approximately 10, 20, 40, and 80 nm, respectively. We estimate a negligible roughness (i.e., ~2 nm) for the 10 nm thick NCL, and therefore we expect that the film grown on such thin layers carries a residual stress similar to that of the film without NCL.

The observation of varying roughness with NCL thickness leads to the conclusion that the critical film thickness at which residual stress buildup begins depends on the NCL thickness. Beyond this critical thickness, stress should increase just as in the film on the bare substrate [Fig. 6(b)]. This trend is clearly in agreement with the data shown in Fig. 3. To substantiate the discussion, we draw in Fig. 3 the expected paths of the stress versus film thickness curves for various NCL thicknesses. If the concept holds, the intercepts of these lines with the vertical at $d=120$ nm should lead to the data (crosses) shown in Fig. 4 (variation of stress at film thickness $d=120$ nm with the NCL thickness). The agreement between this prediction and the actual experimental data (filled squares) is very good.

B. Interface toughening

The purpose of this analysis is to present a justification as to why the film grown on the NCL buckles at larger film stresses (strain energy stored in the film). To this end, we turn to the analysis of the elastic buckling of films on rigid substrates. The film instability occurs when the energy release rate of the advancing delamination front driven by buckling, $G(a)$, is larger than the critical energy release rate of the interface, G_c. This is equivalent to requiring that the ratio

$$\frac{G(a)}{G_c(a)} = \frac{G_0[1-(a_0/a)^2][1+3(a_0/a)^2]}{G_c[\psi(a)]} \tag{2}$$

is larger than unity.[26] Here, a is half the width of the buckle (measured in the direction perpendicular to the direction of the buckling front), a_0 is the initial interfacial flaw size (from which the buckle started), and $G_0=\sigma\varepsilon d/2$, where σ and ε are the residual stress and strain in the film. The critical energy release of the interface G_c is a function of the mode mixity at the tip of the interface crack or the debonding front. The mode mixity is defined by the phase angle ψ or the arctan of the ratio of applied shear to applied normal (opening) stress in the interface. The phase angle changes with a. $G_c(\psi)$ is a continuously increasing function of ψ and is taken as a property of the respective interface.

For a given film thickness, the numerator in Eq. (2) is identical for the film with and without NCL. This is the driving force for delamination, which depends on the film state (thickness, residual stress) and not on the interface. However, the critical energy release rate G_c should depend on the presence of the NCL.

In the nanostructured interface case, failure of the interface entails the deformation and fracture of the rods. The rod failure is expected to take place at its junction with the substrate or with the film. However, failure is more probable at the interface with the substrate due to the material mismatch there (which does not exist at the junction with the film). Here, we assume that the nanorods deform elastically up to failure. This assumption is rooted in the observation that the yield stress and hardening behavior depend on the size of the specimen at this scale. This size effect entails an increase of the yield stress and hence an apparent strengthening of nanostructures.

Let us consider an isolated nanorod of length L_r and diameter D, which makes an angle α with the substrate [inset of Fig. 7(a)]. A force F making an angle ψ with respect to the normal to the substrate acts on the top end of the nanorod. The two components of F in the direction normal and parallel to the substrate are P and T, respectively. By using the relations $\sigma_i=P\rho$ and $\tau_i=T\rho$, where ρ is the number density of nanorods, the two forces are related to the stress state loading the interface. Then, the phase angle ψ results as $\psi=\arctan(T/P)$. The two stresses σ_i and τ_i load the interface in the opening and shear modes, respectively.

The force F loads the rod in tension and bending. The maximum normal stress in the rod is evaluated using the simple beam theory as[27]

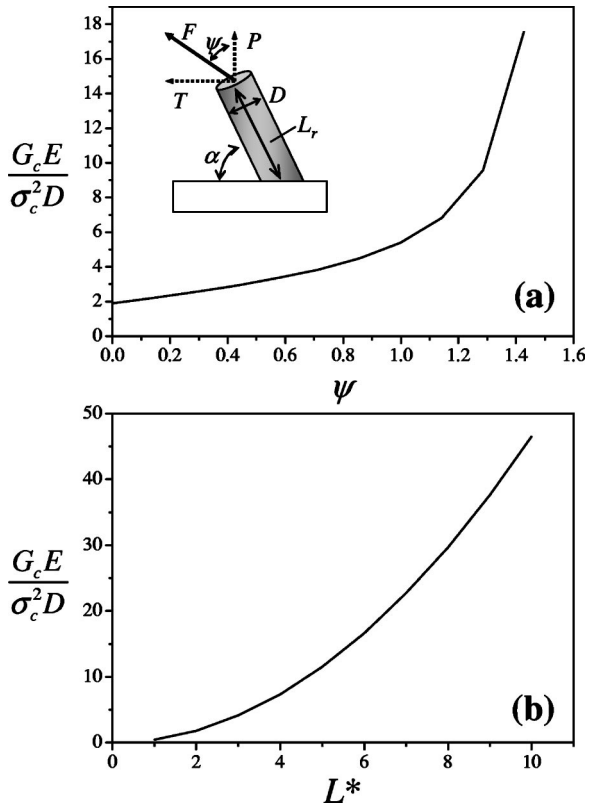

FIG. 7. (a) Normalized critical energy release rate, G_c, for an interface crack propagating along the NCL as a function of the phase angle [Eq. (5) with constant E, σ_c, and D]. The parameters of the NCL are taken $\alpha=50°$ and $L_r^*=L_r/D=3$. The inset shows the definition of the model and its geometric parameters. (b) Variation of G_c with the normalized rod length L_r^*, for $\psi=\pi/4$ and $\alpha=50°$.

$$\sigma_{\max} = P f(\psi,\alpha,D,L_r), \tag{3}$$

where

$$f(\psi,\alpha,D,L_r) = \frac{4}{\pi D^2}\frac{\sin(\alpha+\psi)}{\cos(\psi)} + \frac{32L_r}{\pi D^3}\left|\frac{\cos(\alpha-\psi)}{\cos(\psi)}\right|.$$

This stress is reached at the interface of the rod with the substrate. The rod fails when $\sigma_{\max}$ reaches a critical stress σ_c which is taken as a material constant. The toughness of the NCL may be evaluated as the total work that needs to be done on the rods (per unit area of NCL) up to their failure. This quantity equals the total strain energy stored in one rod at the failure point multiplied by the number density of rods.

The total strain energy stored in a nanorod subjected to P and T is given by[27]

$$w = \frac{2L_r}{\pi E D^2}[P\sin(\alpha)+T\cos(\alpha)]^2 + \frac{32L_r^3}{3\pi E D^4}[-P\cos(\alpha)+T\sin(\alpha)]^2, \tag{4}$$

where E is the Young's modulus of the material of the rod (tungsten). Then, the critical energy release rate may be computed based on the above as

$$\frac{G_cE}{\sigma_c^2 D} = \frac{\rho D^2\left[\frac{2L_r^*}{\pi}\left(\frac{\sin(\alpha+\psi)}{\cos(\psi)}\right)^2 + \frac{32L_r^{*3}}{3\pi}\left(\frac{\cos(\alpha-\psi)}{\cos(\psi)}\right)^2\right]}{\left[\frac{4}{\pi}\left(\frac{\sin(\alpha+\psi)}{\cos(\psi)}\right) + \frac{32L_r^*}{\pi}\left|\frac{\cos(\alpha-\psi)}{\cos(\psi)}\right|\right]}. \tag{5}$$

Here, a superscript "*" represents a normalization with the rod diameter D.

Equation (5) shows that for the given values of E, σ_c, and D, G_c varies linearly with the rod number density, ρ increases nonlinearly with the length of the rod L_r, and increases rather steeply with the mode mixity angle ψ. Figure 7(a) shows the variation of $G_cE/\sigma_c^2 D$ with ψ for $\alpha=50°$ and $L_r^*=L_r/D=3$. These values for α and L_r* are measured from SEM images of the NCL film with $d=50$ nm. The rod number density used here is $\rho=1/D^2$, which corresponds to the situation in Fig. 2 in which the rods are next to each other and the average distance between their axes equals their diameter D.

At this point it is not possible to compare the predictions of Eq. (5) with experimental results from toughness measurements of interfaces with and without NCL. The toughness of the interface without NCL is also expected to be an increasing function of ψ, however, the functional form of this dependence must be established experimentally. This work is ongoing.

Notwithstanding this limitation, this analysis shows that the toughness of the interface in presence of the NCL should be larger than that without the layer. Let us consider a pure opening mode loading of the interface ($\psi=0$). In absence of the compliant layer, the toughness is associated with debonding which also occurs in the case of the NCL at the interface of nanorods and the substrate (when $\sigma_{\max}=\sigma_c$). In the case of the NCL, additional energy needs to be spent to deform the nanorods. Hence, the energy required to open up the NCL interface is larger.

Figure 7(b) shows the variation of $G_cE/\sigma_c^2 D$ from Eq. (5) with the normalized rod length $L_r^*=L_r/D$, for $\psi=\pi/4$ and α 50°. The rapid increase of G_c with the rod length implies that the thicker the compliant layer, the larger the critical film thickness for buckling, which is in qualitative agreement with the experimental observations presented in Figs. 3 and 4.

V. CONCLUSION

In conclusion, it was shown that a nanostructured compliant layer formed by the oblique angle sputter deposition technique and sandwiched between the film and the substrate provides stress reduction, adhesion improvement, and a high critical thickness for thin films. The technique is all *in situ*, does not require any lithography steps, and the nanostructures are made from the same material as the deposited thin film. By using this approach we were able to reduce the stress in sputter deposited tungsten films by approximately one order of magnitude. A model is developed to explain the

origins of the experimental observations and to assist future optimization of the technique.

ACKNOWLEDGMENTS

This work was supported by the NSF. The authors thank D.-X. Ye for taking the SEM micrographs of the samples.

[1]K.-D. Lee, E. T. Ogawa, S. Yoon, X. Lu, and P. S. Ho, Appl. Phys. Lett. **82**, 2032 (2003).
[2]M. J. O'Keefe and S. E. Stutz, Mater. Res. Soc. Symp. Proc. **472**, 233 (1997).
[3]D. C. Meyer, A. Klingner, T. Holz, and P. Paufler, Appl. Phys. A: Mater. Sci. Process. **69**, 657 (1999).
[4]M. D. Kriese and W. W. Gerberich, J. Mater. Res. **14**, 3019 (1999).
[5]G. Zazzara and I. E. Reimanis, Surf. Coat. Technol. **111**, 92 (1999).
[6]H. Maier, J. Luthin, M. Balden, J. Linke, F. Koch, and H. Bolt, Surf. Coat. Technol. **142–144**, 733 (2001).
[7]T. J. Vink, W. Walrave, J. L. C. Daams, A. G. Dirks, M. A. J. Somers, and K. J. A. van den Aker, J. Appl. Phys. **74**, 988 (1993).
[8]A. Bensaoula, J. C. Wolfe, A. Ignatiev, F.-O. Fong, and T.-S. Leung, J. Vac. Sci. Technol. A **2**, 389 (1984).
[9]D. S. Gardner and P. A. Flinn, J. Appl. Phys. **67**, 1831 (1990).
[10]R. R. Kola, G. K. Celler, J. Frackoviak, C. W. Jurgensen, and L. E. Trimble, J. Vac. Sci. Technol. B **9**, 3301 (1991).
[11]A. M. Haghiri-Gosnet, F. R. Ladan, C. Mayeux, H. Launois, and M. C. Joncour, J. Vac. Sci. Technol. A **7**, 2663 (1989).
[12]H. Windischmann, J. Vac. Sci. Technol. A **9**, 2431 (1991).
[13]J. A. Thornton, J. Vac. Sci. Technol. **11**, 666 (1974).
[14]J. A. Thornton, J. Vac. Sci. Technol. **12**, 830 (1975).
[15]J. A. Thornton, Annu. Rev. Mater. Sci. **7**, 239 (1977).
[16]J. A. Thornton, J. Vac. Sci. Technol. A **4**, 3059 (1986).
[17]J. A. Thornton, Proc. SPIE **821**, 95 (1987).
[18]R. Rastogi, V. Dharmadhikari, and A. Diebold, J. Vac. Sci. Technol. A **9**, 2453 (1991).
[19]S. Luryi and E. Suhir, Appl. Phys. Lett. **49**, 140 (1986).
[20]D. Zubia and S. D. Hersee, J. Appl. Phys. **85**, 6492 (1999).
[21]D. Zubia, S. H. Zaidi, S. R. J. Brueck, and S. D. Hersee, Appl. Phys. Lett. **76**, 858 (2000).
[22]T. Karabacak, J. P. Singh, Y.-P. Zhao, G.-C. Wang, and T.-M. Lu, Phys. Rev. B **68**, 125408 (2003).
[23]Y.-P. Zhao, D.-X. Ye, G.-C. Wang, and T.-M. Lu, Nano Lett. **2**, 351 (2002).
[24]K. Robbie, M. J. Brett, and A. Lakhtakia, Nature (London) **384**, 616 (1996).
[25]G. C. Stoney, Proc. R. Soc. London **A32**, 172 (1909).
[26]L. B. Freund and S. Suresh, *Thin Film Materials* (Cambridge University Press, Cambridge, 2004).
[27]F. P. Beer, E. R. Johnson Jr., and J. T. DeWolf, *Mechanics of Materials* (McGraw-Hill, New York, 2002).